

# International Conference on Space Optics—ICSO 2014

La Caleta, Tenerife, Canary Islands

7–10 October 2014

*Edited by Zoran Sodnik, Bruno Cugny, and Nikos Karafolas*



## *Elisa technology consolidation study overview*

*E. D. Fitzsimons*

*N. Brandt*

*U. Johann*

*S. Kemble*

*et al.*



## ELISA TECHNOLOGY CONSOLIDATION STUDY OVERVIEW

E. D. Fitzsimons<sup>1</sup>, N. Brandt<sup>1</sup>, U. Johann<sup>1</sup>, S. Kemble<sup>2</sup>, H-R. Schulte<sup>1</sup>, D. Weise<sup>1</sup>, T. Ziegler<sup>1</sup>.

<sup>1</sup>*Airbus DS GmbH, 88039 Friedrichshafen, Germany*

<sup>2</sup>*Airbus DS Ltd., Stevenage, United Kingdom*

### I. INTRODUCTION

The eLISA (evolved Laser Interferometer Space Antenna) mission is an ESA L3 concept mission intended to detect and characterise gravitational radiation emitted from astrophysical sources [1]. Current designs for eLISA [2] are based on the ESA study conducted in 2011 to reformulate the original ESA/NASA LISA concept [3] into an ESA-only L1 candidate named NGO (New Gravitational Observatory) [4]. During this brief reformulation period, a number of significant changes were made to the baseline LISA design in order to create a more cost-effective mission. Some of the key changes implemented during this reformulation were:

- A reduction in the inter satellite distance (the arm length) from 5 Gm to 1 Gm.
- A reduction in the diameter of the telescope from 40 cm to 20 cm.
- A reduction in the required laser power by approximately 40%.
- Implementation of only 2 laser arms instead of 3.

Many further simplifications were then enabled by these main design changes including the elimination of payload items in the two spacecraft (S/C) with no laser-link between them (the daughter S/C), a reduction in the size and complexity of the optical bench and the elimination of the Point Ahead Angle Mechanism (PAAM), which corrects for variations in the pointing direction to the far S/C caused by orbital dynamics [4] [5].

In the run-up to an L3 mission definition phase later in the decade, it is desirable to review these design choices and analyse the inter-dependencies and scaling between the key mission parameters with the goal of better understanding the parameter space and ensuring that in the final selection of the eLISA mission parameters the optimal balance between cost, complexity and science return can be achieved.

### II. MISSION ANALYSIS

In the baseline orbit for (e)LISA, the three S/C are arranged in an equilateral formation, inclined by 60° to the ecliptic and trailing the earth by approximately 50 Mkm (20°) in a heliocentric orbit. The formation rotates with a period of one year. The orbit, however, is not perfect. Certain effects of Keplerian motion along with perturbations from the Earth, Moon and large planets result in variations in the formation size and shape, typically referred to as 'breathing'. In particular, the operation of the metrology system places limitations on the magnitude of these variations. Four key variations are the breathing angle, the range rate, the point-ahead angle and the arm-length difference. Knowledge of how these factors vary with the formation size is a key component of any future design trade off.

A significant change proposed during the NGO reformulation study was the adoption of a so-called 'drift away' orbit. In the drift away configuration, the S/C are injected into the science orbit closer to Earth (*e.g.* at 30 Mkm). The centre of the formation is then allowed to drift away from Earth over the course of the mission lifetime. The main advantage is a significant  $\Delta V$  saving but this comes at the cost increased orbit perturbations due to the closer proximity of the Earth. This adds an additional parameter; the influence of the starting position on the performance of the orbit.

To assess the influence of these design criteria on the orbit performance, a number of science orbit optimisations were performed, varying certain key orbit design and optimisation criteria, and then computing the main performance indicators for each orbit solution. Specifically:

- The formation arm length was varied from 1 Gm to 3 Gm.
- The initial orbital injection point for the drift away orbit was varied from 30 Mkm to 40 Mkm.
- Optimisation algorithms which target both 2- and 3-arm formations were used.

For all optimisations, a drift away orbit ending at a distance of 60 Mkm after a mission lifetime of 6 years was assumed (60 Mkm being the limit for reliable communications [4]). Note that, there is no principle limit for the mission lifetime, drift-away orbits lasting 10 years, or longer, are feasible. The results are shown in Fig. 1.

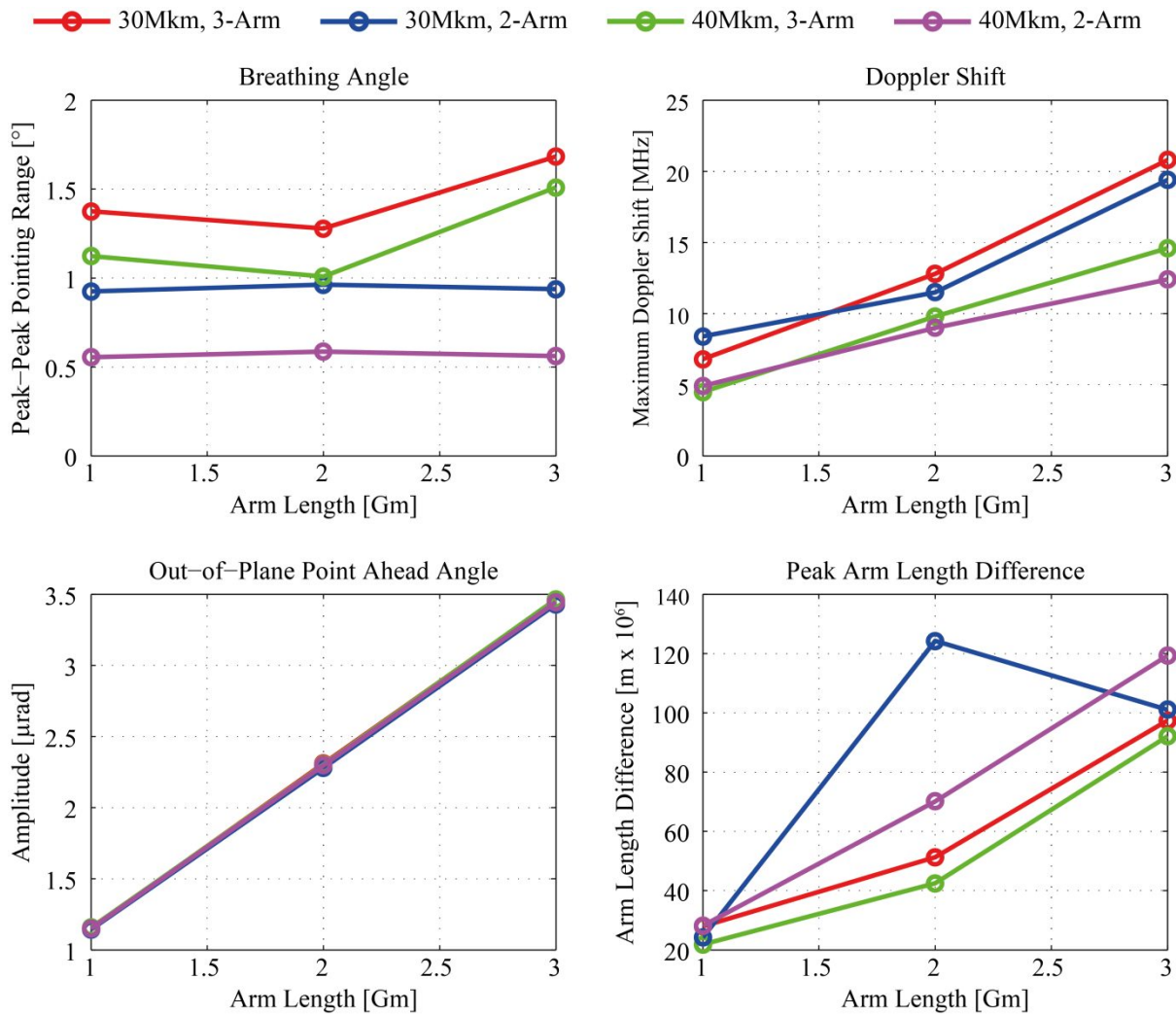


**Fig. 1.** Results showing the dependence of four key orbit performance criteria on formation arm length using different design parameters. The legend for all four plots is shown at the top of the figure.

### A. Breathing Angle

The variation of the breathing angle is shown in the top left panel of Fig. 1. The breathing angle is defined as the peak-peak difference in the inter-arm angle - nominally  $60^\circ$  - which varies over a year as the formation changes. The value used in the figure is the maximum change in pointing over the 6 year mission duration that was considered. The value is significant because the optical metrology system must actively be adjusted to accommodate this variation, either by articulating the entire payload assembly or by utilising a small adjustable mirror within a wide-field telescope (in-field pointing) [6], this places limits on how large a variation can be easily accommodated, and is especially significant in the case of in-field pointing.

From the figure it is clear that there is a small dependence on the breathing angle with arm length. More interesting is the trend with starting position; there is a clear decrease in the breathing angle in orbits which start farther from Earth, confirming that perturbations arising from proximity of Earth are a major driver of this effect. Also interesting is that 2-arm configurations can exhibit significantly smaller breathing angles, this is due to the optimisation algorithm only having to optimise for a single vertex - as opposed to all three vertices for a 3-arm formation.

### B. Doppler Shift

Due to the formation breathing, the relative line-of-sight velocity of the S/C change. This leads to a Doppler shift on the light received by each S/C. Limitations of the photo detection and phase measurement system mean that this cannot be arbitrarily large. Current designs for eLISA hardware can cope with heterodyne frequencies up to 20-25 MHz [7]. The variation of the Doppler shift is shown in the top right panel of Fig. 1. From the

figure we observe a clear linear dependency of the Doppler shift on the formation size. It is also clear that formations starting farther from Earth experience a lower Doppler shift (*i.e.* the Earth is a significant factor in this effect). Two-arm formations may offer lower Doppler shifts but the gain is marginal.

### C. Point Ahead Angle

The rotation of the formation, combined with the finite light travel time between S/C, results in there being a difference between the direction in which laser light is received from the far S/C and the direction in which it must be transmitted to the far S/C to ensure maximum signal to noise, this is called the Point Ahead Angle (PAA). This is typically characterised by a static offset in the in-plane degree of freedom (*i.e.* in the plane of rotation of the formation) and by a periodic variation in the out-of-plane degree of freedom. This out-of-plane variation is more significant as it potentially requires an active correction (as in the case of the PAAM which featured in the LISA design [3] [5]). The amplitude of the out-of-plane variation in the PAA is shown in the lower left panel of Fig. 1. Here it is clear that there is a highly linear dependence of the variation on the formation size, with no significant discernible dependence on any of the other parameters.

### D. Arm Length Difference

The final orbit performance criteria considered is the peak arm length difference. In operation, a Michelson interferometer will be synthesised from the individual laser links of eLISA in a process known as Time Delay Interferometry (TDI) [8]. In order to assure good performance of this technique, the differences in the absolute lengths of adjacent arms should be minimal. The peak round trip arm-length difference is shown in the lower right panel of Fig. 1. Here a roughly linear dependence on the arm length is observed, and some improvement can also be seen in formations which start further from Earth. The point for the 2 Gm, 2-arm formation starting at 30 Mkm (blue line in the figure) is believed to be erroneous, and a result of the nature of the optimisation algorithm which is based on a Genetic approach and does not explicitly use this parameter as a main optimisation criteria.

## III. POINT AHEAD ANGLE MECHANISM

As can be seen from the lower left panel in Fig. 1, the amplitude of the out-of-plane PAA has a highly linear relationship with the formation arm length. In the case of LISA, with 5 Gm arms, this resulted in a maximum PAA variation between the send and receive beams of  $\pm 6 \mu\text{rad}$ , a factor of  $\sim$  two larger than the width of the transmitted beam [3]. In this case, it was clear that some active compensation was required (to prevent total signal loss) in the form of the PAAM [5]. With the reduction of the arm length to 1 Gm in the NGO reformulation, the magnitude of the PAA variation decreased to just over  $\pm 1 \mu\text{rad}$ . Further, the decrease in the telescope size increased the far-field beam width to over  $5 \mu\text{rad}$ , bringing the variation well within the size of the beam. This enabled the removal of the PAAM from the baseline mission architecture, significantly simplifying the optical bench [4]. Considering the case of eLISA, it is prudent to perform a more detailed analysis on the effects of removing the PAAM, investigate how best to compensate for the PAA passively and to investigate how large a formation may be possible without utilising a PAAM.

Note that this analysis exclusively considers the variable out-of-plane component of the PAA. The static in-plane component is well understood and can easily be mitigated during construction and alignment of the optical bench since it is a constant offset.

### A. Accommodation Principle

With no active correction of the PAA, the transmit beam (TX) would be sent along the same direction as the nominal receive beam - the beam which optimally completes the science interferometer with maximum heterodyne efficiency (RX). In the case where there is a non-zero out-of-plane PAA,  $\theta$ , there are then three choices as to how to orient the S/C, illustrated in Fig. 2.

1. Point the beam towards the receiving S/C - the 'TX' vector in the figure. In this case the RX beam will be received at an angle, reducing the heterodyne efficiency at the science interferometer.
2. Point the S/C in the 'RX' direction. In this case, the heterodyne efficiency will be maximised, but the TX beam will be de-pointed from the far S/C, lowering the received power.
3. Point the S/C somewhere in the middle. In this case the RX beam will be received at an angle and the TX beam will be offset from the far S/C, but in both cases by an amount less than in either of the extremes.

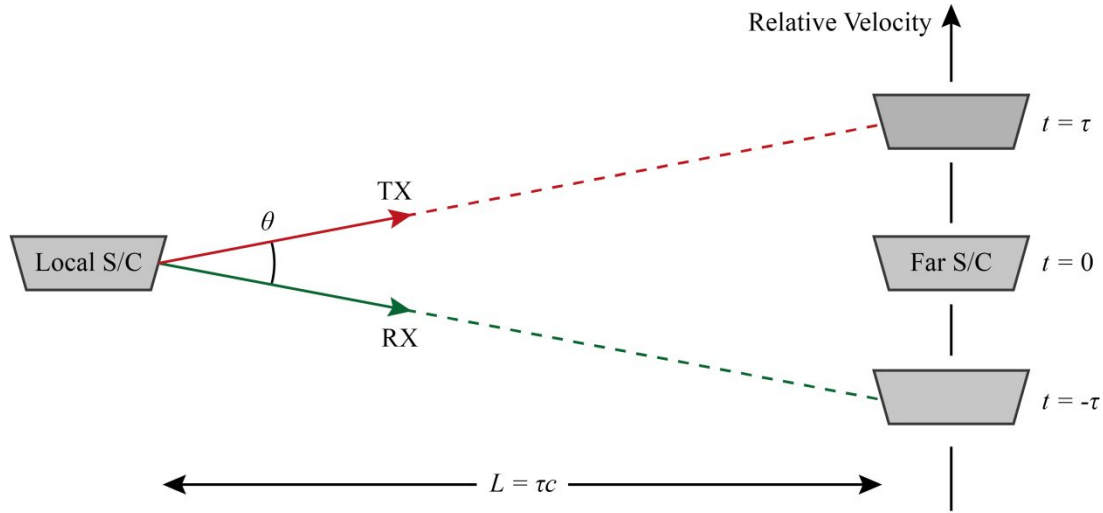


**Fig. 2.** Diagram illustrating the out-of-plane point ahead angle. If there is some relative velocity between the S/C, then over the light travel time,  $\tau$ , the far S/C will move. This means the optimum TX and RX directions will no longer coincide, resulting in a non-zero PAA,  $\theta$ . With a PAAM, TX can be moved with respect to RX, such that perfect pointing is always possible.

The two quantities which are affected - the received power and the heterodyne efficiency - couple to the instrument performance primarily through the shot noise measured in the science interferometer, the main limiting noise source of the metrology. It therefore makes sense to investigate this effect in terms of the overall system metrology noise - nominally  $12 \text{ pm}/\sqrt{\text{Hz}}$  (for a single link) [4].

To investigate which of the three accommodation options outlined above is most suitable, the metrology noise was calculated as a function of S/C tilt. Fig. 3 (left panel) shows the dependency of the received power and heterodyne efficiency on the S/C tilt - in this case for a S/C with a 20 cm telescope and 1 Gm arm length. It can clearly be seen that the received power decreases faster than the heterodyne efficiency with increasing S/C tilt. Extending this calculation, Fig. 3 (right panel) shows the metrology noise as a function of tilt for a variety of arm lengths. This indicates that there is an optimum balanced position, at approximately  $0.23 \cdot \theta$  from TX. Interestingly, the location of this optimum is roughly independent of the formation arm length, and thus also from  $\theta$ . This can be explained by considering that both of these quantities - received power and heterodyne efficiency- are essentially calculated as a double integral over the telescope aperture. The variation with angle is therefore roughly independent of the main system design properties (arm length, laser power and telescope radius).

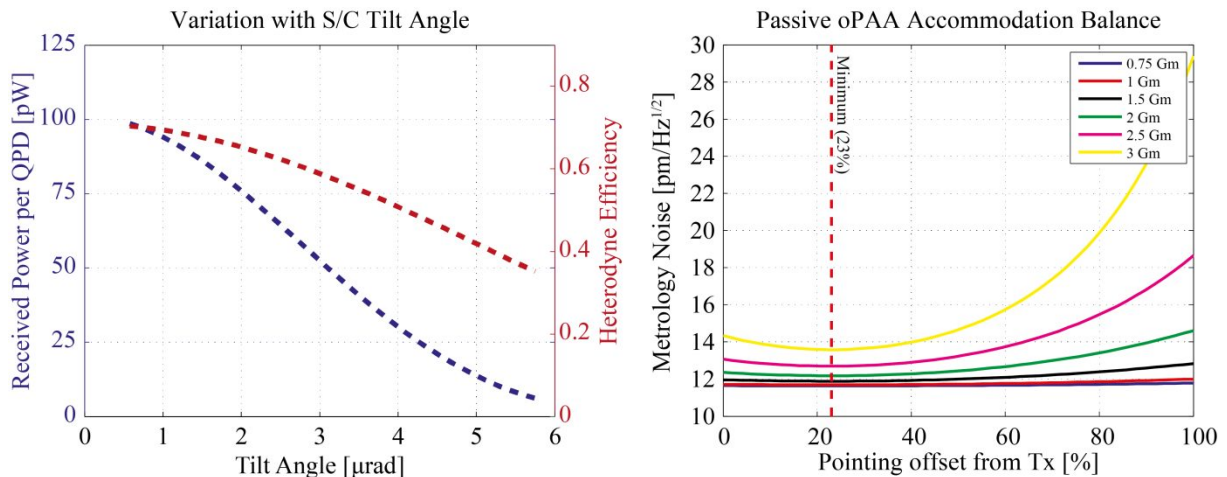


**Fig. 3.** Left: Variation of the received power and heterodyne efficiency with increasing system tilt. Right: Metrology noise as a function of offset from the 'TX' vector, for a variety of formation arm lengths. Since the PAA increases linearly with arm length, the offset has been normalised to 1.

### B. Scaling With Arm Length

In order to calculate the scaling of the effect with arm length, it is necessary to make some assumptions about the two other key system design parameters: the telescope radius and the laser power. (Not doing so results in a large parameter space.) For the purposes of this analysis, it has been assumed that the telescope radius scales linearly with arm length from 20 cm at 1 Gm to 40 cm at 5 Gm - *i.e.* extrapolating between the NGO and LISA configurations. The laser power then scales such that, with no tilt of the S/C, 200 pW of power is received at the far S/C, as per the nominal design [3] [4]. This enables the entire system to be conveniently parameterised as a function of arm length.

Utilising this assumption, the single-link metrology noise can be calculated as a function of arm length. Fig. 4 (left panel) shows the single link metrology noise calculated between 0.5 Gm and 5 Gm, for each of the three accommodation methods outlined above. The resulting strain sensitivity ( $\delta L/L$ ) is shown on the right. As expected, pointing to RX to maximise the heterodyne efficiency results in the largest increase in noise, with the first diffraction minima in the transmit beam visible at around 4 Gm.

Never the less, from the figure, it is clear that passive accommodation of the out-of-plane PAA is feasible at arm lengths in the range of 1 to 2 Gm, and even at 3 Gm only a marginal decrease in performance is experienced.

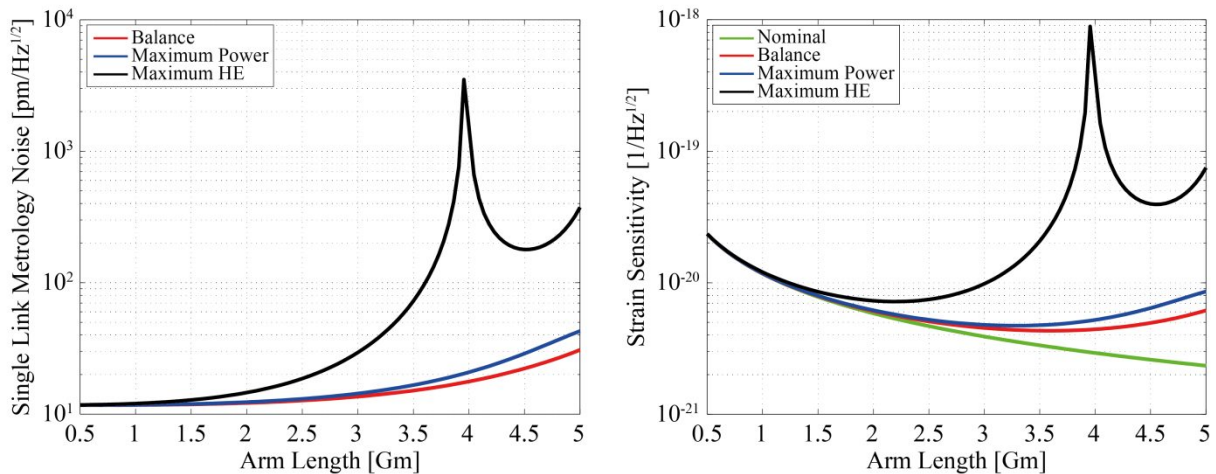


**Fig. 4.** Left: Scaling of single-link metrology noise with arm length for the three passive PAA accommodation methods. Right: Strain sensitivity ( $\delta L/L$ ). The nominal curve shows the strain sensitivity assuming an actively compensated PAA.

## IV. MISSION PARAMETERS

The three top-level parameters which define the mission are the arm length, the telescope radius and the laser power. All three of these parameters directly affect the ultimate strain-sensitivity of the detector. It is thus very important that, as far as possible, we understand dependency of the mission performance on these three parameters. In particular, it is important to ensure that when the final eLISA mission design parameters are selected they represent a good balance between instrument cost and complexity and science return.

It is still advantageous to simplify the analysis a little due to the size of the parameter space. Specifically, the relationship between laser power and telescope radius has been calculated as a function of arm length under two different system constraints:

- At a fixed metrology-limited strain sensitivity of  $1.2 \times 10^{-20} / \sqrt{\text{Hz}}$  - the value from the NGO science requirements [4]
- At a fixed single-link metrology noise of  $12 \text{ pm}/\sqrt{\text{Hz}}$  - the value calculated during the NGO formulation phase and inherited from LISA [3] [4]

Further, in each case, the dependence has been calculated assuming both active (*i.e.* with a PAAM) and passive accommodation of the point ahead angle, as discussed in Section II. The results are shown in Fig. 5 and Fig 6.

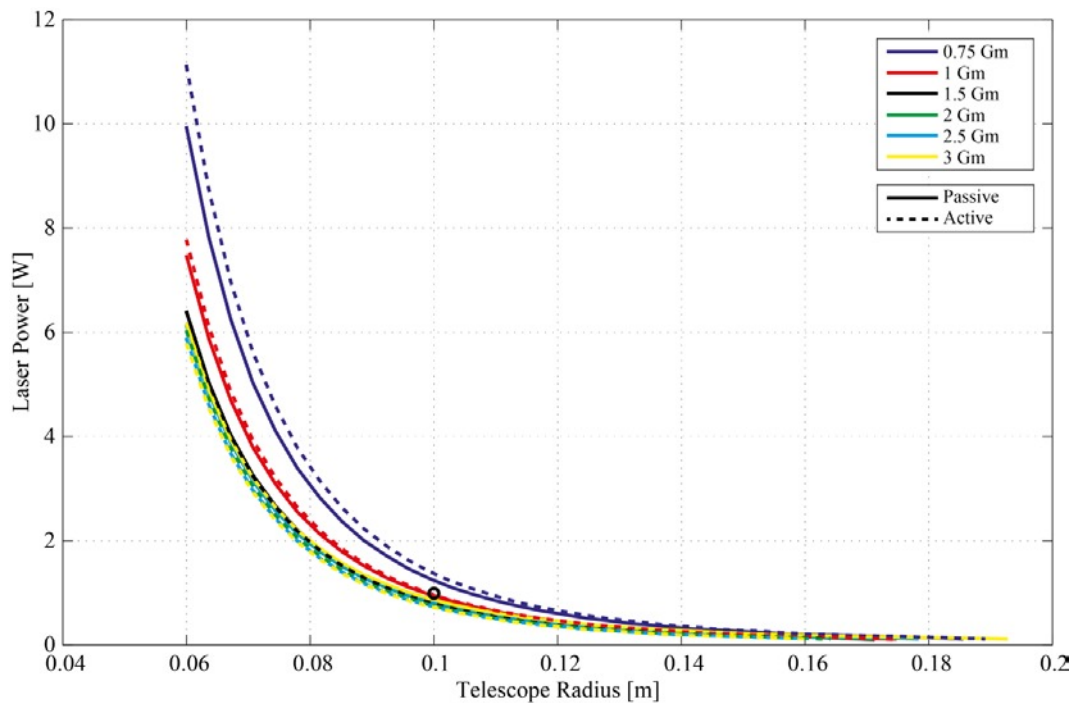


**Fig. 5.** Plot showing the balance between laser power and telescope radius, at a range of arm lengths, under the assumption of a fixed metrology-limited strain sensitivity of  $1.2 \times 10^{-20} / \sqrt{\text{Hz}}$ . Curves assuming both active (dashed) and passive accommodation of the PAA are shown. The black circle denotes the NGO configuration.

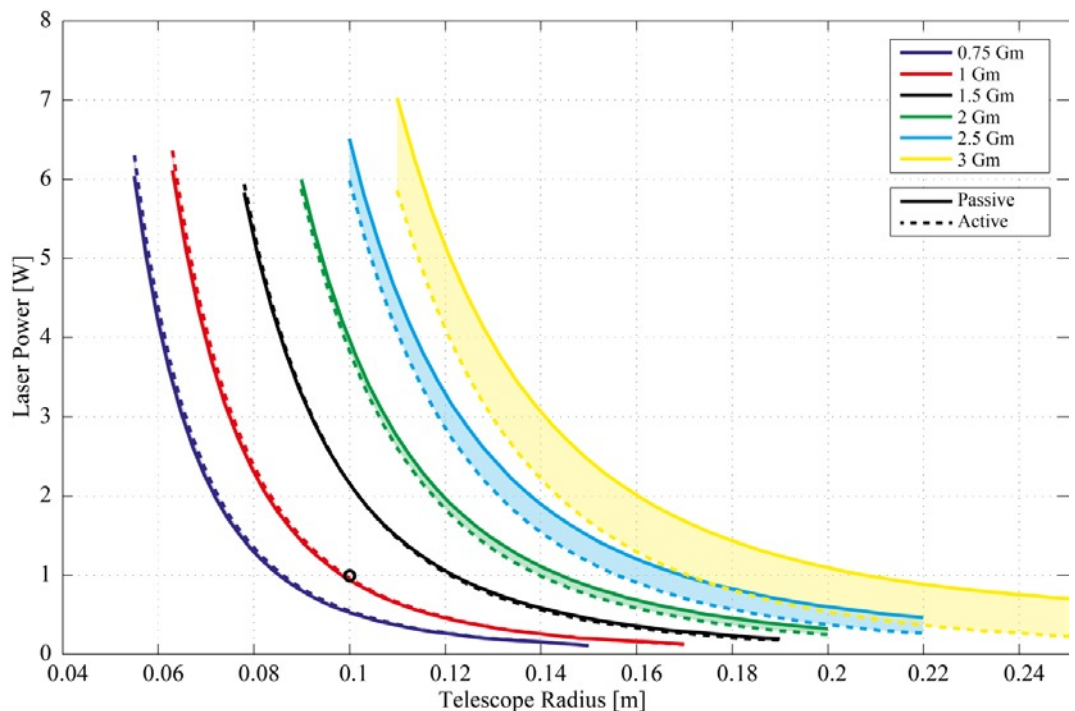


**Fig. 6.** Plot showing the balance between laser power and telescope radius, at a range of arm lengths, under the assumption of a fixed single-link metrology noise of  $12 \text{ pm} / \sqrt{\text{Hz}}$ . Curves assuming both active (dashed) and passive accommodation of the PAA are shown. The black circle denotes the NGO configuration.

It is interesting to note that, from Fig. 5, simply increasing the constellation arm length does not implicitly lead to a significant increase in the metrology-limited strain sensitivity, rather complementary increases in at least one of the laser-power or telescope radius is also required to increase the strain sensitivity. Also, as expected from the analysis in Section II, keeping the metrology noise fixed requires significant increases in laser power or telescope radius in order to utilise passive accommodation of the point ahead angle. It is also interesting to note that, in the case of a 1 Gm formation, the NGO configuration lies close to the knee of the curve,

representing a good balance between laser power and telescope radius for a 1 Gm mission at the required strain sensitivity.

Taking the analysis shown in Fig. 5 and Fig. 6, a selection of case studies demonstrating potential eLISA configurations has been considered as a means of highlighting some of the possibilities. These are summarised in Table 1 and the corresponding strain sensitivity curves for each are shown in Fig. 7. The case studies are restricted to be compatible with the simplifications outlined in the introduction and studied here, such that they could realistically be implemented as ESA-only L3 missions. In particular they all include fully passive accommodation of the point ahead angle.

- Alternate NGO Science: Has the same metrology-limited strain sensitivity as NGO, but requires less laser power
- Science Balance: Possesses improved strain sensitivity compared to NGO, but with only modest increases arm length, laser power and telescope radius.
- Optimal Science: Delivers the best strain sensitivity within the applied constraints

**Table 1.** Case studies to illustrate possible eLISA configurations. The original ESA/NASA LISA configuration and the ESA L1 NGO configuration are included for comparison.

	NGO (ESA L1 configuration)	Alternate NGO Science	Science Balance	Optimal Science	LISA (Original ESA/NASA Configuration)
Arm Length	1 Gm	1.5 Gm	1.5 Gm	2 Gm	5 Gm
Telescope Radius	0.1 m	0.1 m	0.11 m	0.13 m	0.2 m
Laser Power	1 W	0.83 W	1.4 W	1.65 W	1.6 W

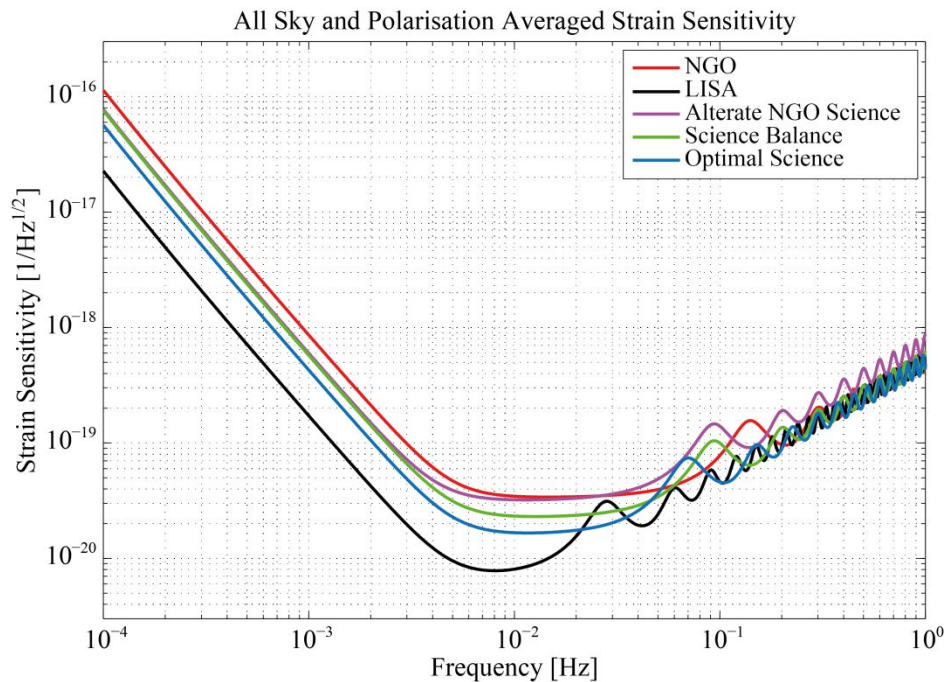


**Fig. 7.** All sky and polarisation averaged strain sensitivity for a variety of possible eLISA configurations and the LISA and NGO reference designs.

The 'Science Balance' and 'Optimal Science' configurations are especially interesting as they offer a significant improvement in strain sensitivity over the NGO design with only modest increases in the key system design parameters. It is also interesting to visualise the dependency of the strain sensitivity on the laser power and telescope radius. Fig. 8 shows, for the 1.5 Gm 'Science Balance' case on the left and the 2 Gm 'Optimal Science' case on the right, how the strain sensitivity reduces as the laser power and telescope radii are relaxed towards the NGO reference design. The main effect is towards higher frequencies, where the sensitivity is dominated by the metrology system and the antenna pattern. Crucially, the key low-frequency part of the spectrum is not affected.

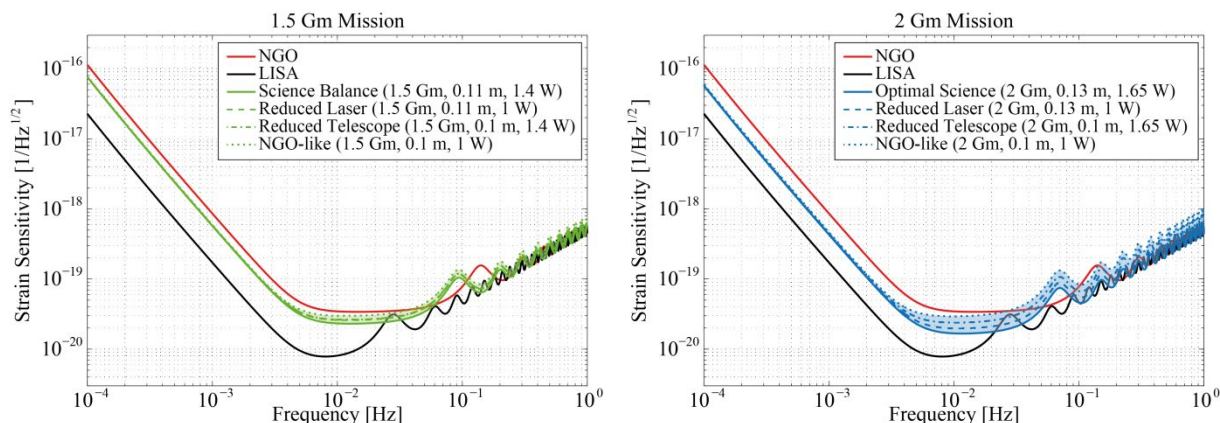


**Fig. 8.** Left: Dependence of the strain sensitivity on the telescope radius and laser power for a 1.5 Gm mission, showing the relaxation of the 'Science Balance' case study towards the NGO reference design. Right: Dependence of the strain sensitivity on the telescope radius and laser power for a 2 Gm mission, showing the relaxation of the 'Optimal Science' case study towards the NGO reference design.

## V. CONCLUSIONS

The key system-level simplifications that were adopted during the NGO reformulation study have been reviewed and found to represent a good compromise between system cost/complexity and performance. Drift-away orbits can offer similar performance to fixed orbits, with similar lifetimes, yet require a lower overall  $\Delta V$  per S/C. Depending on the formation configuration, different orbital design optimisation algorithms can be implemented to provide improved performance in terms of the breathing angle and range range. Missions with arm lengths up to at least 2 Gm (assuming a telescope diameter around 20 to 25 cm) can safely operate without the need for a point ahead angle mechanism, reducing the system complexity and removing a potential single-point failure. Considering the balancing of the top-level design parameters, the NGO configuration represents a reasonable compromise. However, within the constraints of an eLISA mission (that is, one of a similar scale and budget to NGO), it is possible to achieve improved performance compared to the NGO reference design with only modest changes.

## VI. ACKNOWLEDGEMENTS

This work was supported by the German Space Agency, DLR (Deutschen Zentrums für Luft- und Raumfahrt).

## VII. REFERENCES

- [1] P. Amaro-Seoane, S. Aoudia, S. Babak, P. Binétruy, E. Berti, A. Bohé et. al., "Low-frequency gravitational-wave science with eLISA/NGO", *Class. Quantum Grav.* **29** 124016 (2012).
- [2] The eLISA Consortium, "The Gravitational Universe", <http://arxiv.org/abs/1305.5720>.
- [3] The LISA International Science Team, "LISA Assessment Study Report", ESA/SRE(2011)/3, February 2011.
- [4] O. Jennrich, P. Binétruy, M. Colpi, K. Danzmann, P. Jetzer, A. Lobo et. al., "NGO Assessment Study Report", ESA/SRE(2011)/19, December 2011.
- [5] J. Pijenburg, N. Rijnveld and H. Hogenhuis, "Extremely stable piezo mechanisms for the New Gravitational Observatory", ICSO 2012 Proceedings (2012)
- [6] H. Kögel, D. Gerardi, J. Pijenburg, M. Gohlke, Th. Schuldt, U. Johann, C. Braxmaier, and D. Weise, "Interferometric Characterization and Modeling of Pathlength Errors Resulting from Beamwalk Across Mirror Surfaces in LISA", *Appl. Opt.* **52**, 3516-3525 (2013).
- [7] O. Gerberding, B. Sheard, I. Bykov, J. Kullmann, J. Delgado, K. Danzmann and G. Heinzel, "Phasemeter core for intersatellite laser heterodyne interferometry: modelling, simulations and experiments", *Class. Quantum Grav.* **30** 235029 (2013)
- [8] F. B. Estabrook, M. Tinto, and J. W. Armstrong, "Time delay interferometry with moving spacecraft arrays", *Phys. Rev. D* **69**(8), 082001 (2004).